Vortex Formation and Force Generation Mechanisms of the DelFly II in Hovering Flight

A. Tenaglia, M. Percin*, B.W. van Oudheusden, S. Deng and B. Remes
Delft University of Technology, Delft, the Netherlands

ABSTRACT

This paper addresses the unsteady aerodynamic mechanisms in the hovering flight of the DelFly II flapping-wing Micro Aerial Vehicle (MAV). Stereoscopic Particle Image Velocimetry (Stereo-PIV) were carried out around the wings at a high framing rate. Thrust-force was measured to investigate the relation between the vortex dynamics and the aerodynamic force generation. The results reveal that the Leading-Edge-Vortex (LEV), as well as the high flexibility of the wings, have a major effect on thrust generation. Comparison of three wing pairs with different aspect ratio (AR) is also reported, yielding significant differences in both vortical structures and thrust generation.

1 INTRODUCTION

The interest for Micro Air Vehicles (MAVs) is motivated by their versatility and adaptability that make them attractive for a wide range of operations. To be able to carry out these missions, MAVs require great agility and enhanced maneuverability. In this respect, flapping-wing concepts are regarded as promising systems at low Reynolds numbers, considering the abundance of flapping animal species in nature. Over the years, both biologists and engineers have investigated the mechanisms involved in insect and bird flight that may lead to flyer-based solutions for new, innovative MAV designs. In view of the inadequacy of a quasi-steady approach for the analysis of a flapping wing flight, experimental and computational research have brought new insights. There is currently consensus that the dominant aerodynamic mechanisms that govern the performance of a flapping-wing flyer are: 1) [1, 2, 3, 4] *delayed stall* and the presence of a *Leading-Edge Vortex* (LEV) which, entailing lower pressure on the wing surface, produces very high lift coefficients; 2) [5, 6, 7] *rotational circulation* and *wake capture*, mechanisms that are able to produce high peaks in force production during stroke reversal; 3)[1, 3] *clap-and-fling*, a lift-enhancing effect, which takes advantage of the wing-wing interaction at the end of the strokes.

Delft University of Technology (DUT) is represented in this research area with the DelFly, a bio-inspired small-scale ornithoper. The first version of the DelFly was presented during EMAV '05 competition in the summer of 2005. Since that time, research and development of flapping-wing MAVs has continued at DUT.

Figure 1: DelFly II in flight.

The DelFly project follows a top-down approach, which means that by studying a large-scale model, insights can be gained to develop an improved, even smaller, version. The DelFly II (fig. 1) is the object of the current research. It has a biplane wing configuration with the wing structure composed of Mylar foil and carbon rods; the wing span is 280 mm and it weighs 17 grams. A brushless motor with a motor controller, a gear system and a crank-shaft mechanism, drive the wings in their motion. The DelFly is capable of forward and backward flight, as well as stable hovering. It is equipped with an on-board camera, which enables autonomous flight [8]. Investigation on the DelFly, has addressed different technical aspects: aerodynamical [9, 10, 11], structural [12], and the development of an analytical flight-model. Here, we concentrate on the aerodynamic mechanisms of the DelFly. A prominent feature of the aerodynamics of the DelFly is the aforementioned clap-and-fling. However because of the flexibility of the Mylar foil, the fling occurs as a peeling motion, where the wings curve along the chords and smoothly separate until the separation point reaches the trailing edge (TE). Similarly, the clap can be seen as a reverse peel. De Clercq [9] first examined the aerodynamic mechanisms involved in the hovering flight of the DelFly by means of Stereo-PIV in the vicinity of the wings in combination with simultaneous

*Email address(es): m.percin@tudelft.nl

force measurements. She stated that the peel contributes substantially to the lift generation, due to the LEV formation at the onset of the fling. In particular, the leading edge motion during the outstroke is thought to reinforce the LEV generation by increasing the velocity of the fluid moving into the opening gap. Subsequent experiments, carried out by Groen [10], confirmed that the two most important mechanisms responsible for the lift generation on the DelFly are the LEV development and the clap-and-peel effect. The instantaneous three-dimensional wake structure of the DelFly in forward flight regime was investigated by Percin and Eisma [13]. It was revealed that the wake structure is a complex interaction between tip vortices (TVs), TEVs and root vortices (RVs): a U-shaped vortical structure can be clearly seen at several instants during the flapping cycle, and its intensity increases as the reduced frequency ($k = 2fc/U_{ref}$) increases. This is consistent with the research reported by Muijres et al. [14], who revealed the existence of similar structures in the wake of bats.

Following this approach, the current research considers the generation and behaviour of the vortices involved in the DelFly motion, for a hovering flight regime. Using time-resolved Stereo-PIV and force measurements, it will be investigated how the vortical structures evolve and relate this to the force generation by the wings.

2 Set-Up

The experiments were performed in quiescent environment. Before the start of each experiment, the test room was filled with water-glycol-based particles (mean diameter of 1 μm), by means of a SAFEX generator. A simplified DelFly model without tail, servo-controls, batteries and camera, was positioned on a balance structure which incorporates a 6 component force sensor (Nano 17 Titanium ATI Industrial Automation). The force measurements were recorded at a frequency of 10 kHz. Three wing pairs with the same Mylar foil thickness (10 μm) but with different aspect ratio ($AR = b^2/S$) were tested: 1) a standard wing pair (AR=1.75) with a wing span (R) of 280 mm and a max chord length (c) of 88 mm, 2) a high aspect ratio wing pair (AR=2) with a wing span of 320 mm and the same max chord length, 3) a low aspect ratio wing pair (AR=1.5) with a wing span of 240 mm and the same max chord length. Henceforth they will be referred to as *Std*, *HARDA*, and *LARDA*, respectively. *Std* was scaled up and down in the spanwise direction for the design of *HARDA* and *LARDA*, respectively. The stiffeners were placed with their rear tips at the corners of the wing taper and their front tips at the same relative spanwise position. Since previous experiments near the wings [9, 10] had suffered from the reflection caused by Mylar foils, the wings were sprayed with a mat black paint. This indeed improved the quality of the raw acquired images, although it did not completely eliminate the reflection problem. Two different flapping frequencies (9 and 11.2 Hz) were investigated, but in the current paper only the 11.2 Hz case will be discussed.

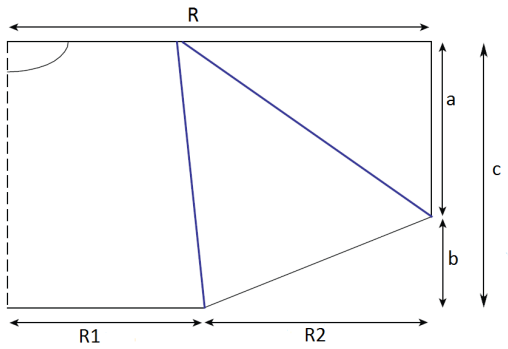

Figure 2: DelFly wing layout.

High-speed Stereo-PIV measurements were carried out at several chordwise-aligned planes around the wing (fig. 3). The first plane was placed at a distance of 40 mm outboard from the fuselage (normal to the laser sheet) and after every recording the complete balance-DelFly system was shifted by steps of 20 mm with respect to the laser sheet. Three CMOS

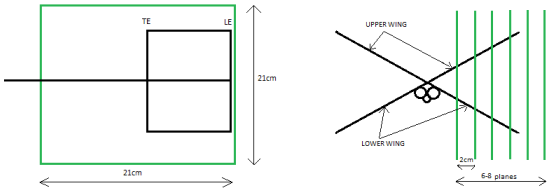

Figure 3: Schematic side view (left) and front view (right) of the measurement configuration.

cameras (High Speed Camera 6 LaVision) with a resolution of 1024x1024 pixels and equipped with a Nikon 60 mm focal objective, were used to record images. The first camera was viewing normal to the object plane, while the others were placed on the same horizontal plane, symmetrically with respect to the focal axis of the first camera, with an angle of 80 degrees between them (thus 40 degrees between each of them and the first camera). These two cameras were also equipped with Scheimpflug adapters. The choice of using three cameras for a stereoscopic approach provided the possibility of capturing both the structure within the wings and outside them during the fling phase, which otherwise would be impossible using only two cameras due to the shadows and visual obstruction by the wings. A field of view of 210x210 mm was captured with a magnification factor of approximately 0.09. Double frame image sequences of tracer particles were recorded with a frequency of 200 Hz, with a time separation between frames varying between 250 and 350 μs. The flow was illuminated with a double pulse Nd:YLF laser (Quantronix Darwin Duo) with a wavelength of 527 nm; thanks to an appropriate setting of lens and mirrors the laser

sheet was able to illuminate the entire region of interest with a thickness of 2 mm. Davis 8.2.0 software was used to control the laser and camera setting, perform image analysis, post-process and display data. The double frame images were interrogated using windows with a final size of 64 x 64 pixels and an overlap of 75%.

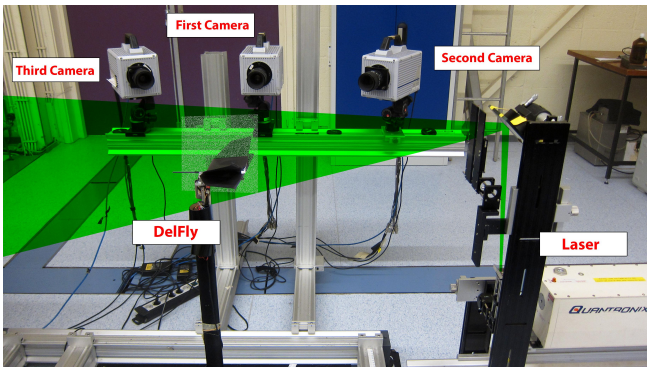

Figure 4: View of the complete set-up.

3 Results

The aim of the current research is threefold: 1) to reveal the generation and subsequent shedding of the vortices from the wings of the DelFly, 2) to relate the vortex dynamics to the thrust measurements (i.e. the force component parallel to the fuselage of the DelFly) and 3) to make a comparison between the three different wing pairs.

3.1 Analysis of vortex dynamics

In this section the general vortical structure will be firstly described for the Std-wing case. By overlapping the PIV-processed vector fields with the corresponding image recordings of the second camera, it is possible to investigate the vortex behaviour while at the same time visualizing the position and shape of the wings. Different phases in a flapping cycle for a plane at 10 cm from the root are reported in the following. The vortices are labelled in order to better follow their trend throughout the images: each label reports the typology (LEV or TEV), the stroke phase (*IN* or *OUT*, for in-stroke or outstroke) and the wing to which they belong (*T* or *B*, for top or bottom). The black bands mask the regions affected by the shadow of the wings: the lack of illumination in these regions makes the evaluation of a velocity vector field unreliable. Other issues regarding the presentation of the results need to be mentioned as well. First of all, due to the presence of the force sensor, the lower region is much more affected by reflection than the upper one, and this impacts the correct representation of the velocity vectors in this region. Secondly, because of the dihedral angle, the laser sheet doesn't illuminate the wings at the same nominal spanwise position (Appendix A): this may cause that the position of vortical structures may occasionally seem to be uncorrelated

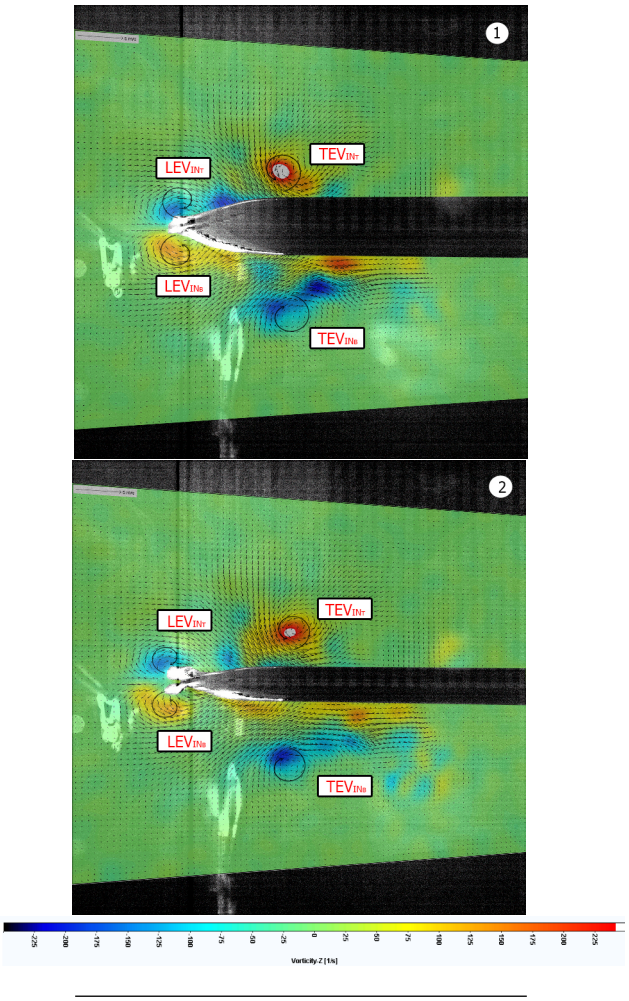

Figure 5: Two different moments of the clap mechanism. Plane located at 10 cm from the root in spanwise direction. Flapping frequency: 11.2 Hz. Time separation between images: 0.005 sec.

between the two wings. For the sake of simplicity, henceforth only the structure of the upper wing will be discussed (unless mentioned otherwise).

In Figs:5,6 four different moments of the clap-and-peel phase are presented. Starting from the top picture of Fig:5, it can be clearly seen that there are two vortices at the start of the clap, labelled as LEV_{IN_T} and TEV_{IN_T}, generated during the instroke. While the LEV_{IN_T} is still attached to the wing, the TEV_{IN_T} seems to be just shed into the wake. It then moves slowly backwards, until it is not anymore possible to track it because of the masked region (bottom picture of Fig:6). The LEV_{IN_T}, instead, moves around the leading edge and it is shed forwards: there it encounters the counter-rotating vortex from the lower wing (LEV_{IN_B}), and they presumably annihilate each other. During the initial instants of the oustroke (Fig:6), air swirls around the leading edges and rolls up into

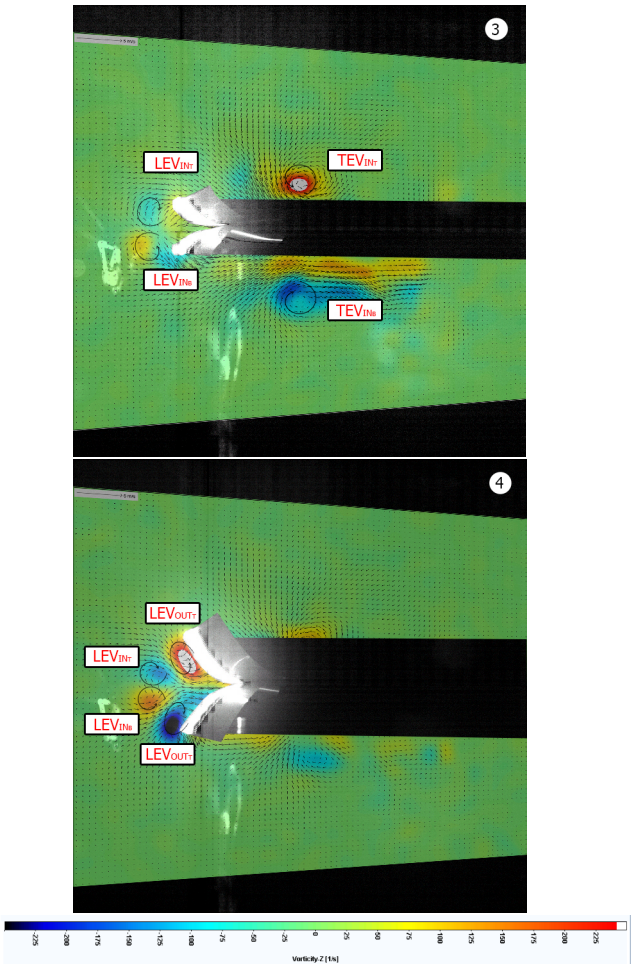

Figure 6: Two different moments of the peel mechanism. Plane located at 10 cm from the root in spanwise direction. Flapping frequency: 11.2 Hz. Time separation between images: 0.005 sec.

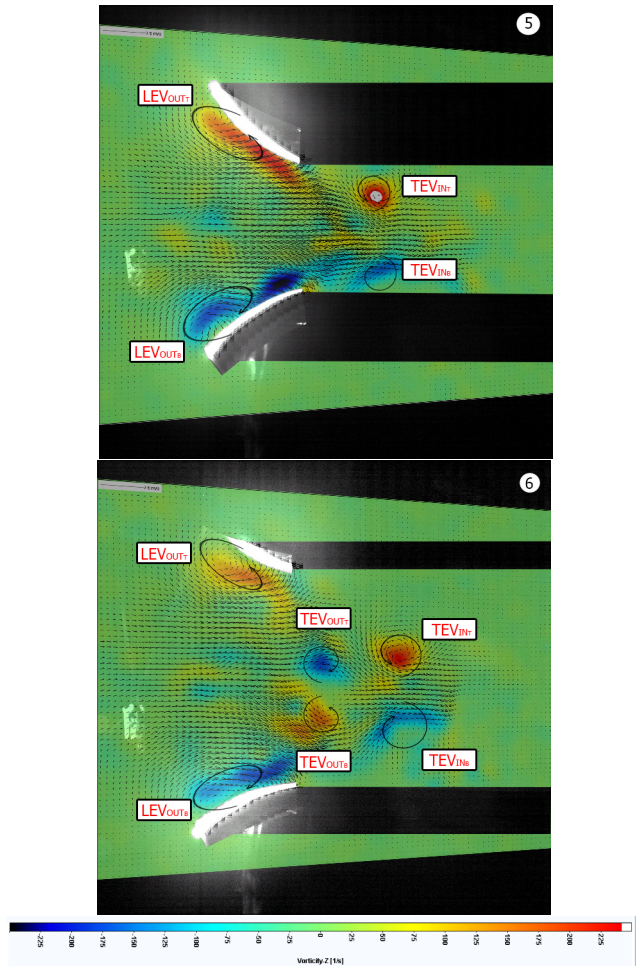

Figure 7: Two different moments in the flap cycle during outstroke. Plane located at 10 cm from the root in spanwise direction. Flapping frequency: 11.2 Hz. Time separation between images: 0.01 sec.

two intense LEVs (LEV_{OUT_T} and LEV_{OUT_B}); as a consequence, an air inrush is clearly visible in the cleft between the wings. The more the wings move away from each other (Fig:7), the more air between them acquires induced velocity and momentum because of the presence of the two vortices. The thrust experienced by the wing can be then interpreted both as a reaction to the time rate of change of this momentum and a suction force applied on the inner side of the wing itself. Approaching the end of the outstroke (Fig:7) it is again possible to see the TEV (TEV_{IN_T}) shed during the previous instroke, which still slowly moves backwards. Also (bottom picture of Fig:7), as soon as the trailing edge starts rotating around the leading edge, a new TEV (TEV_{OUT_T}) is shed into the wake (the latter will diffuse quickly and it will not be visible anymore after the start of the new instroke).

Comparing the results from different planes reveal that the general vortex behaviour briefly described so far is uniform and consistent along the wing span. However, it is worth to mention two important features that have been recognised only in the vicinity of the root, thus on the planes located at 4 and 6 cm. In Fig:8 are reported three different phases of the clap-and-peel mechanism on the plane positioned at 6 cm from the root. The TEV_{IN_T} shed during the clap soon divides into two different TEVs (labelled as TEV_{IN_T} and TEV'_{IN_T}): the TEV'_{IN_T} moves upwards and seems to disappear at the beginning of the peel, while the TEV_{IN_T} behaves like the one previously described for the plane located at 10 cm from the root. Although the cause of this separation is not yet clear, one may speculate how this phenomenon might affect the wake structure and the forces generation. However, this issue is not a topic to be debated in this paper and it will be discussed in future reports. The other feature to be men-

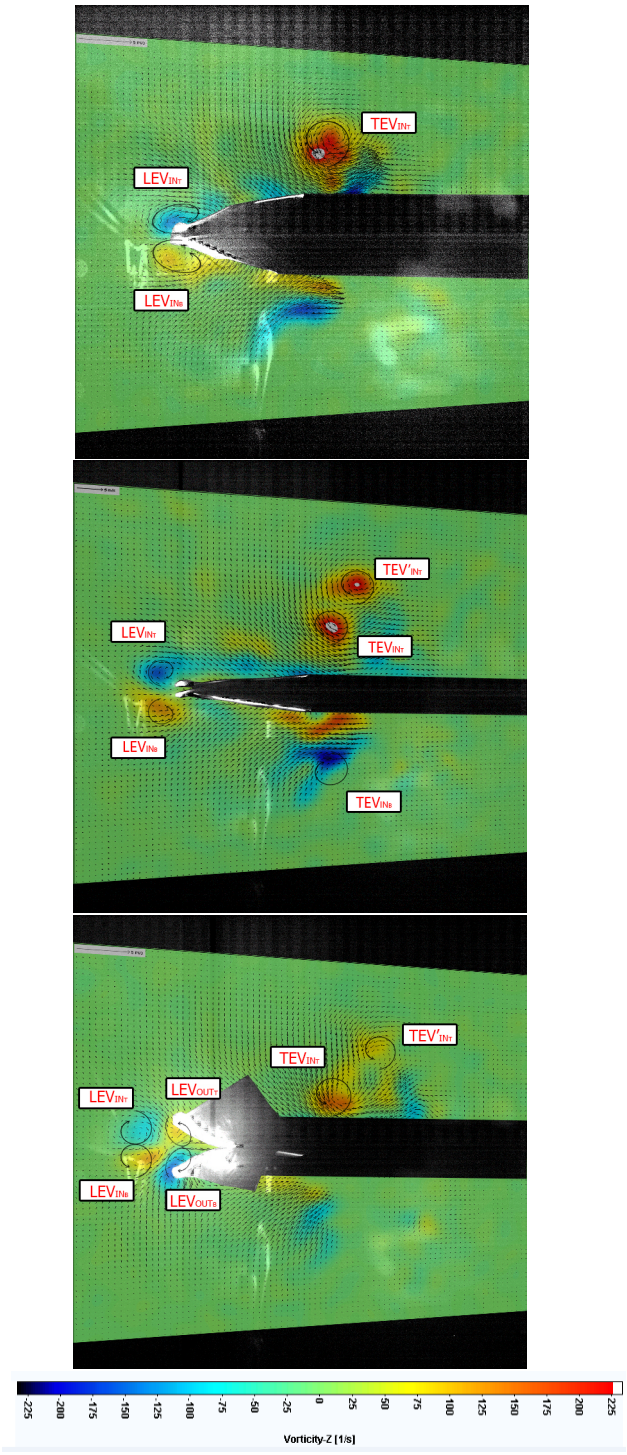

Figure 8: Three different moments of the clap-and-peel mechanism. Plane located at 6 cm from the root in spanwise direction. Flapping frequency: 11.2 Hz. Time separation between images: 0.01 sec.

tioned concerns the behaviour of the TEV_{OUT_T}. A comparison between Fig:9 and the bottom picture of Fig:7 provides a clear evidence that this vortex is no longer present in the wake of the Delfly at this spanwise position. The reason may be related to the shorter distance and a delayed separation between the trailing edges during the peel: both these effects seem to nullify the formation of the TEV_{OUTS}.

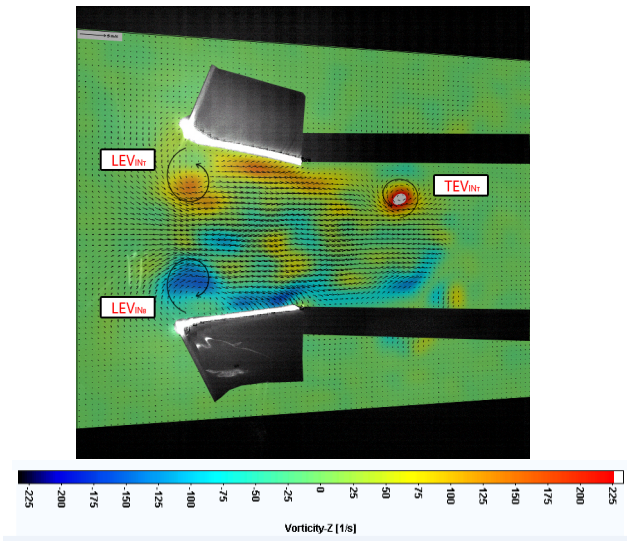

Figure 9: End of the outstroke. Plane located at 6 cm from the root in spanwise direction. Flapping frequency: 11.2 Hz.

Moving towards the tips of the wings, the laser sheet illuminates the wings only when they touch each other, thus only at the clap. For all the other phases, it is then possible to see only the vortical structures shed during the clap, while we lose sight of the vortices that remain attached to the wings. This supports the hypothesis that the TEVs (TEV_{IN_T} and TEV_{IN_B}) are shed during the clap and that they move backwards keeping the same spanwise position throughout the whole flapping cycle. Fig:10 describes behaviour at the end of the outstroke, for the plane located at 14 cm from the root. An analysis of the position of the cores of the TEV_{IN_T} and TEV_{IN_B} from 6cm to 14cm (Figs:9,7,10, respectively), reveals how these vortices are inclined to get closer to each other when approaching the wing tip. This finding suggests that there is a continuous complex structure (a TEV-tube) which is shed from the trailing edges at the clap and which is connected at the tip presumably by a tip vortex, TV.

3.2 Generation of forces

Thrust (viz. lift) is the force in the direction parallel to the fuselage of the DelFly that keeps it aloft in hover. The measured time variation of thrust over two flapping periods is shown in Fig:11 for the considered wing geometries for the flapping frequency of 11.2 Hz. The force data was filtered by means of a Chebyshev Type II low-pass filter. The cut-

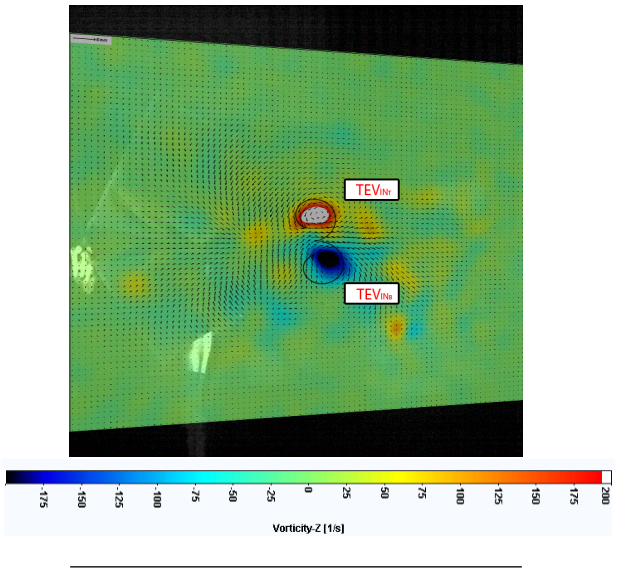

Figure 10: End of the outstroke. Plane located at 14 cm from the root in spanwise direction. Flapping frequency: 11.2 Hz.

off frequency was selected based on the flapping frequency to allow the first two harmonics of the force oscillations to be included in the resultant data as these modes were found to be related aerodynamic forces, as verified by flapping tests carried out under vacuum conditions [10]. Forces are complemented with the variation of the stroke angle (black line), flap-averaged forces and the number labels 1-6 indicate the instants when the PIV images (given in Figs: 5-7) were recorded. The start of the period defined based on the Hall sensor input and corresponds to approximately middle of the instroke.

The reciprocating nature of the flapping motion of the DelFly wings results in the formation of two peaks in the flap cycle with relatively greater thrust generated during the outstroke thanks to the enhancing effects of the clap-and-peel motion. This relative difference becomes more prominent with increasing span length of the wing (20% for LARDA, 36% for Std, and 41% for HARDA). The clap-and-peel motion starts with the approach of the wings at the end of instroke (Fig:5-1). The minimum force is generated approximately at the instant when the wings surfaces are roughly parallel to each other (Fig:5-2) and the leading edges just start the stroke reversal. At this phase, although the LEV_{INT}s are present in front of the wings, the lack of vertical wing area results in diminished force generation. Thrust rapidly increases with the start of the peel motion due to inrush of the fluid into the gap between the wings and formation of the LEVs (Fig:6-3 and 4). Force generation peaks at the middle of the outstroke (presumably when the wings have the largest deformation and thus highest effective angle of attack) and it starts decreasing with the deceleration of the wings and separation of the trailing edges (Fig:7-5 and 6).

Comparison of the mean thrust over the flapping cycle reveals that force generation increases with increasing span length, which might be attributed to the larger area of the wing surface moving with a higher velocity towards the wing tips. Thus, formation of an extended LEV in the spanwise direction with a greater circulation closer to the wing tips probably occurs and enhances the force generation. Logically, the mean power consumption also increases with the change of the span length (1.22 W for LARDA, 1.66 W for Std, and 1.84 W for HARDA).

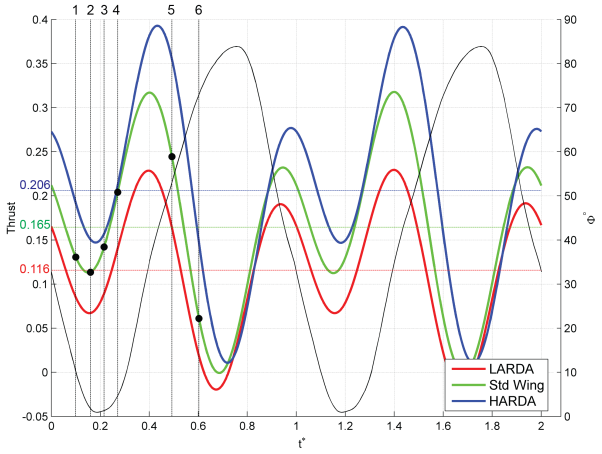

Figure 11: Time variation of thrust plotted for two periods of the flapping motion at the flapping frequency of 11.2 Hz for different wing geometries complemented with the variation of the stroke angle (black line).

3.3 Comparison between different wing pairs

In the previous section, a general description of the vortex behaviour has been presented for the Std-wing case. As shown in Fig:11, both HARDA and LARDA experience a similar thrust variation over the cycle, and, accordingly, they display the same vortical structures. Nevertheless, there are some noteworthy differences. In order to explain them, the plane at 10 cm from the root is considered, which corresponds to 83.3% of LARDA's span and 62.5% of HARDA's span, respectively.

In Fig:12 an instantaneous picture of the clap shows the velocity vector field for HARDA (top figure) and LARDA (bottom figure). It clearly shows the presence of the LEV_{IN_T} and the TEV_{IN_T}, whose behaviour was already described for the Std-wing case in 3.1.

The first anomalous feature is observed for HARDA-wing case: even if the laser sheet is 10 cm far from the root, the break up of the TEV_{IN_T} into two separate vortices (TEV_{IN_T} and TEV'_{IN_T}) is still present. It is likely that this behaviour is a peculiar feature of the region *relatively* close to the root, and that, as a consequence, it strongly depends on the wing

span. The latter statement is also strengthened by the fact that this TEV-split mechanism is hardly visible at 6 cm from the root for LARDA-wing case (figure not reported), where it is instead well-defined for Std-wing and HARDA cases. Moreover, it shows the presence of a vortex (labelled as LEV'_{IN_T}) in clockwise rotation, just below the TEV'_{IN_T} (top picture of Fig:12): its origin and its effect on the TEV-tube (it might be the cause of the split of TEV_{IN}) still need to be further investigated. The peel (Fig:13) confirms that the same vortical structure described before, also occurs for both HARDA and LARDA.

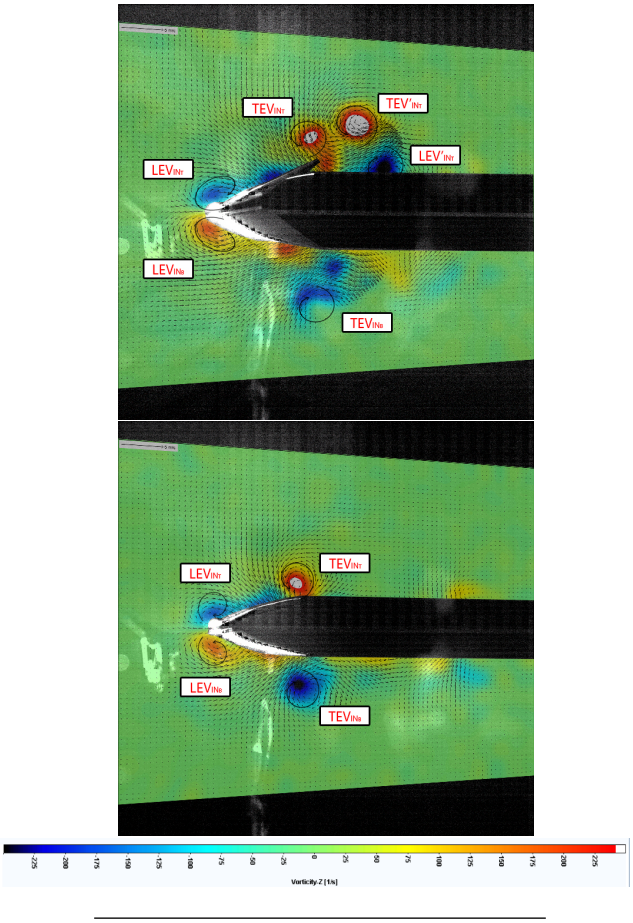

Figure 12: Comparison between HARDA (top) and LARDA (bottom), during the clap. Plane located at 10 cm from the root in spanwise direction. Flapping frequency: 11.2 Hz.

4 Conclusion

The Leading-Edge-Vortices (LEVs) developed during the hovering flight of the DelFly II have been shown to be strongly connected with the thrust generation. Thanks to the flexibility of the wings and to a delayed motion of the trailing-edges with respect to the leading-edges, the angle of attack of the wings reaches high values during both instroke and outstroke. This effect, combined with the existence of attached

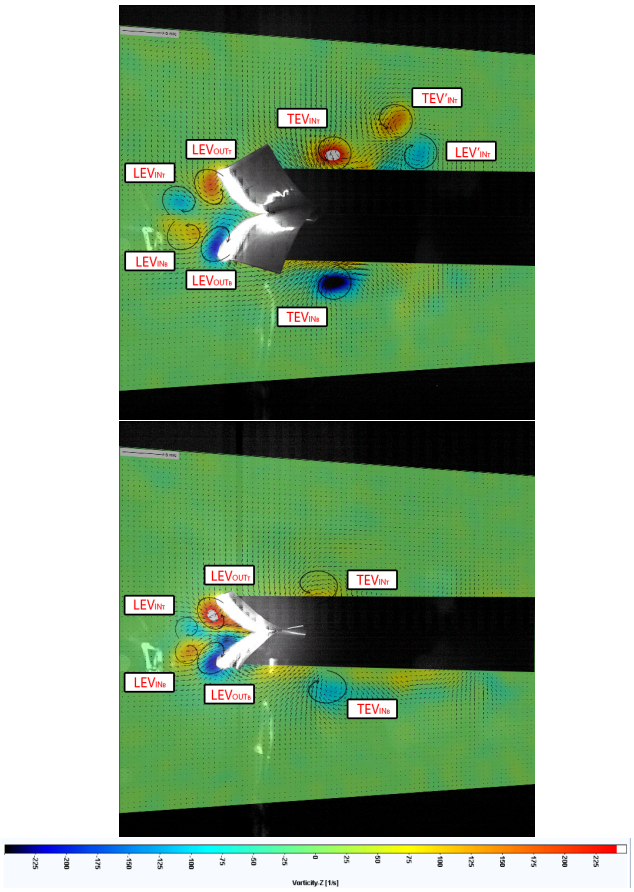

Figure 13: Comparison between HARDA (top) and LARDA (bottom), during the peel. Plane located at 10 cm from the root in spanwise direction. Flapping frequency: 11.2 Hz.

LEVs, yields strong generation of thrust-force. In contrast, because of the absence of these, the thrust-force reaches minimal values immediately after the stroke reversals. Also the Trailing-Edge-Vortices (TEVs) evolution has been hinted, but additional analysis is needed to better clarify their importance in the wake structure and force generation. Finally, a comparison between three wings with different Aspect Ratio (AR) suggested the fundamental role of the latter in forces production.

References

[1] C.P. Ellington. The aerodynamics of hovering insect flight. iv. aerodynamic mechanisms. *The Royal Society*, 1984.

[2] C.P. Ellington, C. van den Berg, A.P. Willmott, and A.L.R. Thomas. Leading-edge vortices in insect flight. *Nature*, 1996.

[3] S.P. Sane. The aerodynamics of insect flight. *The journal of Experimental Biology*, 2003.

[4] W. Shyy and H. Liu. Flapping wings and aerodynamic lift: the role of leading-edge vortices. *AIAA Journal*, .

[5] S.P. Sane M.H. Dickinson, F.O. Lehmann. Wing rotation and the aerodynamic basis of insect flight. *Science*, 1999.

[6] F-O. Lehmann. The mechanism of lift enhancement in insect flight. *Naturwissenschaften*, 2004.

[7] F-O. Lehmann, S.P. Sane, and M. Dickinson. The aerodynamic effects of wingwing interaction in flapping insect wings. *The journal of Experimental Biology*, 2005.

[8] G.C.H.E. de Croon, K.M.E. de Clercq, R. Ruijsink, B. Remes, and C. de Wagter. Design, aerodynamics, and vision-based control of the delfly. *Internation Journal of Micro Air Vehicles*, 2009.

[9] K.M.E. De Clercq. Flow visualization and force measurements on a hovering flapping-wing mav 'delfly ii'. Master's thesis, DUT, 2009.

[10] M.A. Groen. Piv and force measurements on the flapping-wing mav delfly ii. Master's thesis, DUT, 2010.

[11] J. Eisma. Flow visualization and force measurements on a flapping-wing mav delfly ii in forward flight configuration. Master's thesis, DUT, 2012.

[12] B.Bruggeman. Improving flight performance of delfly ii in hover by improving wing design and driving mechanism. Master's thesis, DUT, 2010.

[13] M. Percin, H.E. Eisma, J.H.S. de Baar, B.W. van Oudheusden, B. Remes, R. Ruijsink, and C. de Wagter. Wake reconstruction of flapping-wing mav delfly ii in forward flight. In *International Micro-Air-Vehicle Conference (IMAV)*, 2012.

[14] F.T. Muijres, L.C. Johansson, R. Barfield, M. Wolf, and A. Hedenstrom G.R. Spedding. Leading edge vortex improves lift in slow-flying bats. *Science*, 2008.

APPENDIX A EFFECT OF THE DIHEDRAL ANGLE.

For all the measurements, the laser sheet is normal to the horizontal plane (see Fig:3) and its position is calculated as the distance from the root on a line (black dotted line in Fig:14) parallel to the horizontal plane. As a consequence of the flapping motion, the laser sheet does not illuminate the wing at the same position throughout the flapping cycle. Hence, in order to calculate the exact position, it must be taken into account the offset due to the stroke angle (α). Also, because of the dihedral angle (β), there will be a disparity of the laser position between the two wings. This disparity can be calculated as follows:

$$x_1 - x_2 = \frac{X}{cos(\alpha + \beta)} - \frac{X}{cos(\alpha - \beta)} \qquad (1)$$

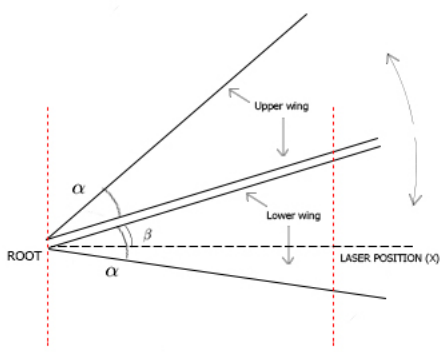

Figure 14: Effect of the dihedral angle on the effective laser sheet position on the wings.

where X is the nominal laser position, x_1 is the laser position on the upper wing, x_2 is the laser position on the lower wing and $x_1 - x_2$ is the disparity of the laser position between the two wings.